A Novel and Comprehensive Single Terminal ANN Based Decision Support for Relaying of VSC Based HVDC Links

Ricardo C. Santos [1]*, Simon Le Blond [2], Denis V. Coury [3], Raj K. Aggarwal [2]

[1] Center of Engineering, Modelling and Social Science, Federal University of ABC, Av. Dos Estados, 5001, CEP 09210-580, Santo André, SP, Brazil

[2] Department of Electronic and Electrical Engineering, University of Bath, Bath, BA2-7AY, United Kingdom.

[3] School of Engineering of São Carlos, University of São Paulo, Av. Trabalhador São-carlense, 400, CEP 13566-590, São Carlos, SP, Brazil.

* ricardo.santos@ufabc.edu.br

Abstract: HVDC technology is increasingly important for long distance bulk power transmission, but existing protection relaying techniques for such a system are subject to limitations. This paper presents a novel Artificial Neural Network (ANN) based on an algorithm for fault detection, location and classification in VSC-HVDC systems. Taking advantage of the ability of ANNs to identify and classify patterns, the proposed algorithm is able to detect and correctly classify a fault occurring at either the rectifier substation on the DC line or at the inverter substation. Therefore, such a scheme can be used as a decision support tool or as a backup protection. Only local signals are used at the rectifier substation and no communication link is necessary, thus improving the system's protection reliability and reducing the overall cost of the hardware implementation. A detailed VSC-HVDC system is described and used to simulate a number of fault scenarios in the system. Using the resulting fault waveforms, a comprehensive decision support scheme is developed and described, paying particular attention to the signal processing chain and design of the specific ANNs for each relaying task. Finally, a detailed analysis of the influence of key fault parameters on the limits of the algorithm's performance is carried out.

Index Terms—Artificial neural networks, fault detection, HVDC transmission, pattern recognition, power system protection, relay.

1. Introduction

Currently, High Voltage Direct Current (HVDC) transmission systems are the best option to transfer a large amount of power over long distances. The advantages are: the ability to interconnect asynchronous systems; fewer losses compared to High Voltage Alternating Current (HVAC) systems; improvements in power system stability; smaller

power towers; and a narrower transmission corridor meaning less rights of way. In spite of the technical, economical and environmental advantages, HVDC systems pose many challenges for power protection engineers as the transient behaviour of very long DC lines and complex terminal converter stations should be modeled to study the system's post fault response.

In order to safely operate HVDC systems, it is important to detect and clear any fault which occurs in the HVDC system as soon as possible [1] – [3]. For this purpose, the most common HVDC protection systems are based on the travelling wave theory [4] – [10], the DC voltage level [11] and differential voltage measurement [12] techniques, the rate of voltage change technique [13] and the current differential scheme [1] – [3],[13]. The rate of voltage change and DC voltage level techniques are normally used as a main protection to detect single phase faults. However, some problems can arise concerning high resistance or multi-phase faults [4] – [6]. Conventional current differential schemes are commonly used as a backup protection, but they are affected by the capacitance of long lines. In addition, they require a communication link and the information must be synchronized between the two ends [14]. Travelling wave based methods still experience problems concerning their practical application since they are very dependent on the high sampling rate, and are therefore difficult to implement, even in hardware. Moreover, this method can be easily influenced by noise [6], [7], [11].

In an attempt to overcome all the aforementioned challenges, researchers are working on novel methods to protect HVDC systems. The method presented in [4] is based on symmetrical components and travelling waves for fault classification and faulty pole selection. Reference [5] describes a new transient harmonic current protection scheme to identify the type of fault. This method uses the DFT to extract information from both terminals of the DC transmission line. In [6] and [7], a hybrid method is shown combining travelling waves and a boundary protection scheme for bipolar HVDC lines. This method was implemented and evaluated in real time using programmable logic devices. Research carried out in [8] presents a new scheme for fault location based on the natural frequency of a distributed parameter line model. In this proposal, only currents from the sending terminal are used and the natural frequency is obtained by the PRONY algorithm. A method for fault location also based on the travelling wave theory is

presented in [9], where Discrete Wavelet Transformation is applied to the voltage and current signals only at the relay terminal and the fault location can be estimated in a segmented HVDC transmission line. The scheme presented in [10] uses a method based on distance protection to enhance the fault distance estimation for faults nearest the remote terminal, and is able to distinguish internal faults from external faults.

As the protection relay of HVDC systems presents complex problem spaces, an alternative approach is to use Artificial Intelligence [15], more specifically Artificial Neural Networks (ANNs) [16] – [23]. Such techniques are appropriate when the conventional approaches do not appear as an effective solution. Most of them describe methods using a pre-processing stage coupled with a Multi Layer Perceptron (MLP) neural network [16] - [19], but significant variations on this theme exist, including using adaptive linear neurons [20], radial basis function neural networks [21] and ANNs optimized by the particle swarm theory [22]. Still considering MLP neural networks, a scheme to detect and classify faults in a HVDC line, presented in [23], should be highlighted. It is important to note that this scheme is only able to operate for DC faults, by using a very high sampling rate, which makes it more complex to implement. Furthermore, cases considering different fault resistances and non-nominal conditions were not considered. As will be discussed later, the solution proposed in the current paper overcomes these limitations.

The work herein presents a solution based on ANN, specifically a feed forward MLP to support the protection scheme of the whole HVDC system, i.e., the rectifier substation, the DC transmission line, and the inverter substation. It is important to highlight that the main focus and contribution of this paper is to clarify and discuss some different possibilities to improve the protection scheme of HVDC systems using ANNs. In addition, it is shown how the outputs of several ANNs, each designed for different purposes, can be combined together with logic gates to improve the robustness and extend the overall protection of the algorithm's operational range.

In order to develop ANNs and evaluate the proposed algorithm, a VSC-HVDC system is modeled and simulated in MATLAB Simulink's Power System Blockset (PSB). A large number of fault cases were generated by varying different fault locations, types of fault, fault resistances and power across the DC transmission line. This paper is

organized as follows. In Section 2, the VSC-HVDC system used is presented and its settings and characteristics are discussed. In Section 3, the proposed algorithm is described in detail. In particular, the training process, pre and post processing and ANN validation criteria are included. In this section, the algorithm is evaluated regarding the training space and signals from PSB/Simulink. In Section 4, the limits of the proposed algorithm are evaluated and a study about accuracy and response time is presented. Finally, the conclusions are drawn in Section 5.

2. VSC-HVDC System Model in PSB/Simulink

Fig. 1 shows the single line diagram of the VSC-HVDC system used in this work to generate a wide range of fault cases. The output waveforms were used to generate RMS values to be used in the ANN training process and to evaluate the final algorithm's performance. This system was modeled and validated in MATLAB [24] and it is essentially representative of a symmetric monopole configuration with Neutral Point Clamped (NPC) and 12-pulse converters on both the rectifier and inverter sides. The nominal voltage at the DC link is ± 100 kV and the rated transmission power is 200 MVA. Regarding the AC sides, both operate with a nominal voltage of 230 kV (50 Hz) and the short-circuit power is 2000 MVA. More details about the used VSC-HVDC system are included in the Appendix, where Fig. A.1 and Fig. A.2 present the AC systems connected at buses 1 and 2, respectively. Similarly, Fig. A.3. and A.4 present the AC and DC filters connected at the rectifier and inverter side, respectively. Table A.1 shows the VSC-HVDC parameters.

To model the distributed nature of the line's parameters more closely, the original "π" model 75 km length DC transmission line was replaced by a DC transmission line with 40 "π" sections, which is sufficient to accurately represent a DC transmission line of 200 km length [25], used in this work.

As can be seen in Fig. 1, the whole system consists of AC equivalent sources, AC and DC filters, capacitors, phase and smoothing reactors and a data acquisition system, only at the rectifier substation. At bus 1, the RMS AC voltages (Va, Vb, and Vc) and the values of the voltage and current (Vd and Id) of the faulted pole in the DC line are available. It is important to highlight that the proposed decision support scheme only uses these available RMS values and DC quantities, provided by existing meters. Vd and Id

are averaged to give the mean values of the voltage and current (Vd and Id) over the last 20 ms, equivalent to one cycle at 50 Hz. It is assumed that the data acquisition system is supplied with AC and DC transducers with sufficient bandwidths. Once the algorithm developed here uses RMS AC values and time averaged DC values, this is a realistic assumption since the transducers only need to provide an accurate response up to the AC system frequency.

In terms of fault types and fault locations on the AC side, all common fault configurations are simulated. On the DC side, only pole-to-ground faults are simulated, because pole-to-pole faults can only be caused by sufficient physical damage to bring the conductor poles together and, therefore, they are very rare [2]. In addition, [26] states that pole-to-pole faults on the DC cables are considered unlikely if the two poles are laid in separate cables with some distance in-between.

3. Proposed Algorithm Based on ANN

The main concept behind this proposal is to use the ANN classification and pattern identification capability to support the protection scheme of the HVDC system presented in Section 2. Signals are collected at the rectifier substation and processed by the algorithm providing a mechanism to generate a trip signal or any other pre-defined control actions. Fig. 2 shows all the input signals used by the algorithm, as well as the processing steps involved. The main part of the algorithm is an ANN using RMS three phase values and DC quantities to detect the operational condition of the HVDC system. To develop this task, four different kinds of ANNs are considered, as follows:

1) ANN to detect a fault;
2) ANN to identify the fault section;
3) ANN to classify a fault at the rectifier substation;
4) ANN to classify a fault at the inverter substation.

Firstly, the algorithm's performance is evaluated regarding each ANN operating separately. This will be followed by a discussion on combining the ANN outputs with logic gates to extend the algorithm's application. Fig. 3 shows the ANNs used in this work, highlighting that all the ANNs take the same input signals and have the same three layer topology, with the exception of the output layer: 100 – 20 – (1, 3 or 7).

A sampling rate of 4 kHz is used to acquire signals at the rectifier substation and five data windows (Va, Vb, Vc, Vd, and Id) of 20 samples each are applied to the ANN input. Thus, each ANN receives the same input vector with 100 inputs and they work independently from each other. It is important to emphasize that after detailed analysis, it was concluded that an ANN using a sample rate of 4 kHz and data windows of 20 samples offered the best performance for the proposed algorithm. Such a sampling rate also makes the overall algorithm relatively easy to implement in hardware and software. Whilst the algorithm could be implemented with an FPGA [6], [27], it is also well within the capabilities of the DSP chips in modern numerical relays.

It is important to note that different ANN topologies were evaluated and the chosen one was the smallest, which was successful in the training process for all ANNs. Furthermore, data windows of 80, 40, 20 and 10 samples were considered, but regarding accuracy and computational burden, the data windows of 20 samples presented the best performance.

The choice of the aforementioned ANNs is entirely based on the ability of ANNs to identify and classify patterns. In turn, the proposed scheme should be able to detect, locate and classify faults at any place in the VSC-HVDC system, since the input signals change for different types and fault locations, as exemplified in Fig. 4. As shown, depending on the type and fault location, the input signals present different behavior before and after a fault so that the ANNs can make a decision about the HVDC operational condition. To make this decision properly, the ANNs continuously receive voltage and current samples (each 250 μs) by moving data windows.

3.1 Pre-Processing Step

A simple pre-processing step is used to form the input vector with the five data windows required, using RMS and DC quantities. When a new sample is acquired, all data windows are updated with the newest sample and the oldest one is discarded. Therefore, when a fault occurs, new samples from the HVDC system under fault go from the rectifier substation to the pre-processing step and data windows containing voltage and current short circuit samples are now used by the ANN. In this situation, the ANN should change its output offering information about the HVDC system.

Mathematically, the pre-processing step is presented in (1) – (4), where k is the latest sample, M is the data window size, i.e., 20 samples in this case, Va is the RMS phase A voltage at bus 1, $\overline{Va}$ is the normalized RMS phase A voltage, Vd is the mean voltage value of the DC line, $\overline{Vd}$ is the normalized mean voltage value of the DC line, Id is the mean value of current through the DC line, and $\overline{Id}$ is the normalized mean value of current through the DC line. The normalization process considerably improves the ANN performance and is based on a suitable choice of base values as will be discussed in Subsection 3.4. Regarding the AC quantities, only phase A is presented, as phases B and C are treated identically.

$$\left[\overline{Va}_{(k)} \cdots \overline{Va}_{(k-M+1)}\right] = \frac{\left\{Va_{(k)} \cdots Va_{(k-M+1)}\right\}}{V_{base}^{AC}} \tag{1}$$

$$\left[\overline{Vd}_{(k)} \cdots \overline{Vd}_{(k-M+1)}\right] = \frac{\left\{Vd_{(k)} \cdots Vd_{(k-M+1)}\right\}}{V_{base}^{DC}} \tag{2}$$

$$\left[\overline{Id}_{(k)} \cdots \overline{Id}_{(k-M+1)}\right] = \frac{\left\{Id_{(k)} \cdots Id_{(k-M+1)}\right\}}{I_{base}^{DC}} \tag{3}$$

$$\begin{aligned} Input\ Vector_{(k)} = \Big[&\overline{Va}_{(k)} \cdots \overline{Va}_{(k-M+1)}\ \overline{Vb}_{(k)} \cdots \overline{Vb}_{(k-M+1)}\ \overline{Vc}_{(k)} \cdots \\ &\overline{Vc}_{(k-M+1)}\ \overline{Vd}_{(k)} \cdots \overline{Vd}_{(k-M+1)}\ \overline{Id}_{(k)} \cdots \overline{Id}_{(k-M+1)}\Big]^T \end{aligned} \tag{4}$$

3.2 Artificial Neural Networks (ANNs)

With reference to Fig. 3, each ANN receives the same input vector from the preprocessing step. Depending on the task each ANN was designed for, the relevant output neuron is then trained to change output from -1 to 1 to indicate detection of a positive fault condition. For example, for the ANN in Fig. 3(b), the output vector [-1 1 -1] indicates a fault in the DC line. Thus, using the ANNs shown in Fig. 3, it is possible to detect the fault, identify the section under fault and classify the fault.

The classification task for AC faults beyond the rectifier and inverter substations is different. As will be discussed later, the phases involved in any fault occurring at the

rectifier substation can be accurately classified as the measurements are made locally. However, for AC faults occurring beyond the inverter substation, only the type of faults can be identified, i.e., single-phase, double-phase or three-phase. In this case, no specific information about the phases can be identified due to the converters between the relay and the fault and the similarity between the pre and post fault conditions, mainly for high fault resistance values.

3.3 Counter Function

An independent counter was connected to each ANN output to avoid any unstable response. It generates a trip signal only after a predefined number (N) of consecutive ANN outputs higher than a threshold value (V). Otherwise, the counter is reset and the counter output remains at level 0, which prevents false trips due to noise or any other transient condition in the power system. Both parameters N and V can be changed to fine tune the algorithm's response without the need for ANN retraining, as will be shown later.

3.4 ANN Training Process

The training process seeks to provide the ANN with enough knowledge to robustly conduct a specific pattern recognition task and, therefore, is a vital step in the development of the proposed algorithm. As is well known, a representative training set must capture the full range of possible pre and post fault VSC-HVDC operational conditions. Therefore, a careful study was undertaken to determine the best training set size for this application, showing that 4,346 input vectors were the most suitable choice.

The training set was built from 53 different operational cases of the system presented in Fig. 1. From each new case, 21 pre-fault and 61 post-fault input vectors were acquired, resulting in 4,346 input vectors [(21+61)×53]. To generate each particular case, the simulation was executed under a different condition, i.e., one of the following parameters was changed:

1) Type of fault at the rectifier or inverter side (single-phase, double-phase or three-phase);

2) Fault location on the DC line (0, 50%, and 100%);

3) Fault inception angle (0º, 45º, and 90º);

4) Fault resistance (0, 5 Ω, 10 Ω, 15 Ω, and 20 Ω);

5) Power across the line MVA (0.7 pu, 0.8 pu, 0.9 pu, 1 pu);

6) Voltage magnitude at the Thevenin equivalent of the AC system at bus 1 (0.9 pu, 0.95 pu, 1 pu, and 1.05 pu).

It is important to note that the training set did not include all possible combinations, but instead a sample of 53 cases was chosen to accurately represent the boundaries of the problem space.

The training set used to train the ANN fault detection is presented in Fig. 5, where each input vector is defined according to (1) – (4). When an input vector is related to a pre-fault condition, all the ANNs in Fig. 3 are trained to an output equal to -1, but when an input vector is related to a post-fault condition, only the relevant output neuron is trained to an output equal to 1. The training set purposefully did not include input vectors that had pre and post fault data together, which could make this process infeasible.

Before training the ANN, the training set should be normalized, as the neurons at the input layer only work effectively with values ranging between -1 and 1. Therefore, three base values were defined for the normalization process, which makes the training process more efficient and it improved the algorithm performance. The base values defined are respectively the highest elements of AC RMS, Vd and Id present in the training setting, shown in Fig. 5. These values are called respectively V^{AC} base, V^{DC} base and I^{DC} base and they were used in the normalization process, but also in the pre-processing step as shown in (1) – (3).

As mentioned earlier, this ANN is an MLP type with a hyperbolic tangent activation function in the input and hidden layers and a linear activation function in the output layer, which is suitable for applications involving pattern recognition and classification tasks [15]. The Backpropagation algorithm was used to perform a supervised learning training process, which is a typical choice when using ANN in power systems [16] – [23]. The main training parameters used in this work are:

- Momentum: 0.9;
- Learning rate: 0.01;
- Desired error (minimum error): $1x10^{-9}$;

- Maximum number of iterations: 500,000;
- Learning procedure: Batch.

3.5 Algorithm's Validation Process

To validate the proposed algorithm, forty new operational situations were executed using PSB/Simulink and applied to ANN inputs following the pre-processing step. The same parameters described in Section 3, Subsection 3.4 (items 1 to 6), were used to generate cases different from those used in the training process. In the context of ANNs, it could be called a Generalization Test. However, not only is the ANN output analyzed, but also the overall algorithm's response time as power system protection is a time critical application.

Table 1 shows 40 test cases used in this work. Each case's parameters are shown compared to the respective response times, where V_{AC1} and P are in pu, and R_F is in Ohms. The Detection Time (T_D), Location Time (T_L), Rectifier Classification Time (T_{CR}) and Inverter Classification Time (T_{CI}) are respectively the response time in ms related to the ANN output presented in Fig. 3. The fault inception angle is not presented due to the fact that when using the AC RMS values, its effect is not significant in the final result. The times presented in Table 1 include the delay generated by the counter and represent a completely stable and reliable response.

Table 2 presents *N* and *V* for each ANN output and Fig. 6 (a) illustrates the ANN output and the counter output for case 21, presented in Table 1 and Fig. 2. Furthermore, Fig. 6 shows the response time analysis for each specified ANN from Fig. 3, under different fault conditions presented in Table 1. It can be seen that the counter ensures that the algorithm issues a decisive response only after the ANN output stabilizes. For all cases, the simulation time was 3 s and the fault was always applied between 1.5 s and 2.5 s. It is important to highlight that the main purpose of Fig. 6 is to show how each ANN works, i.e., as can be seen, only the expected ANN output ranges from -1 to 1, while the other outputs do not change, remaining at -1.

As summarized in Table 1, it can be observed that the response time for faults at the inverter side is longer than in all the other cases. Therefore, whilst this algorithm would be viable as a main protection or logical support for the rectifier side and DC line,

it should be restricted to backup protection (or logical support) for the inverter side. In terms of an integrated protection scheme, it is a very interesting application, whereby the whole system is protected by the same hardware with the same robust and fault-tolerant technique (ANN) and without any communication link, i.e., operating only with local signals. An improvement is expected in the protection system reliability when the amount of cables, the number of different hardware and monitoring signals are reduced. As shown in Fig. 7, only available signals are used to protect/monitor the whole HVDC system and no new infrastructure is needed, which means it is inexpensive to implement. Moreover, as the proposed scheme is designed to be used as a backup protection or logical support, its response time is not as strict as the main protection response time. It makes the proposed scheme suitable to be implemented in hardware, even using generic hardware platforms available on the market. As highlighted, no additional devices or communication links are needed.

As shown in Table 1, the algorithm failed to detect a single-phase fault before a double-phase fault for case 8. The next subsection explores a way to overcome this drawback and improves the algorithm performance for faults at the inverter side. In this case, “performance” is defined as the algorithm's ability to correctly respond to normal and fault conditions, as well as its response time following a fault.

3.6 Improving the Algorithm’s Performance

To improve the algorithm’s performance concerning faults at the inverter side, the approach reported in this subsection uses three independent ANNs to classify faults, instead of only one ANN with three outputs, as discussed before. Thus, in this approach each ANN has a specific function, as follows: a) ANN to detect single-phase faults; b) ANN to detect double-phase faults; c) ANN to detect three-phase faults. All of them have the same topology, identical to the one shown in Fig. 3(a). The same input training set discussed in Subsection 3.1, as well as the output vector adjusted depending on the ANN’s designated task is used. Specifically, the output vector for the ANN responsible for single-phase faults was trained to 1 only for inputs related to a single-phase fault case and -1 otherwise (even for double-phase or three-phase faults at the inverter side). The same procedure was used for the other two ANNs, and consequently three completely

exclusive ANNs were developed. It should be highlighted that this new proposal is now formed by six ANNs and not only four ANNs, as previously shown in Fig. 3.

The new scheme was tested using the same forty cases initially used (see Table 1) and the results are presented in Table 3. The last column still has the response time T_{C1} obtained for the first approach (one ANN with three outputs), allowing a direct performance comparison between both approaches. It is important to note that the response time for single-phase faults was increased to 10 ms, however for double-phase and three-phase faults this time was reduced. Nevertheless, the most significant impact is the correct classification of case 8, which is explained by the fact that it is an ANN specially used for classifying single-phase faults. The adjustments of parameters N and V used in each ANN output are presented in Table 4. These parameters are chosen to meet the worst fault case, which can be found by analyzing all the simulation results.

4. Evaluation of Algorithm Limits

As discussed in the previous section, the algorithm performance is very promising, as it robustly and quickly produced the required output for forty new fault cases. However, these test cases all exist within the limits of the training set range whereas practical, real world conditions could present fault parameters that lie outside of this range. By using the same presented training set generation methodology to extend the training set, the algorithm's range could be improved. However, this could result in prohibitively long training times or larger ANNs topologies. This section, therefore, intends to show the real limits of the algorithm, i.e., identify the fault conditions where each ANN fails.

The methodology to find the limits of the algorithm is based on the following steps:

a) To identify the most critical case for each type of fault, considering the forty cases initially used. This is assumed to be the case with the slowest response time, i.e., for the three-phase fault at the rectifier side, the worst case is 31 (Table 1).

b) For each critical case selected, to change the parameters to generate cases outside of the training range. This can be done by doing the following: 0.85 pu < V_{AC1} > 1.05 pu, P < 0.7 pu, R_F > 20 Ω.

c) Systematically adjust these parameters to produce new test cases until the ANN fails. This is assumed to be the limit of the algorithm.

This procedure quantified the difference between the limits of the training set and the real limits of the algorithm (ΔV_{AC1}, ΔR_F, and ΔP). As shown in Fig. 8, it is important to note that the applicability of the proposed scheme increases the larger the ΔV_{AC1}, ΔR_F, and ΔP are. New tests considering cases outside the training range (item b aforementioned) define a new "real working space". It is a relevant issue to be considered when applying the proposed scheme (methodology) to protect different VSC-HVDC systems.

Table 5 shows the results for 126 new simulated cases, defining ΔV_{AC1}, ΔR_F, and ΔP. A comparison is made between the different ANN performances, as well as the same operational condition. Specific ANNs are also compared to different operational conditions.

4.1 Three-Phase Fault at the Rectifier Side

After 12 new simulations for each ANN, it was observed that R_F does not have any influence on the algorithm performance. Indeed, the performance was affected by P, regardless of the ANN considered. It is important to note that until P = 0.65 pu, the NN_1 (detection) works with an average time for responding T_A = 15.92 ms, i.e., about ¾ of cycle. Moreover, it can be seen that NN_2 (location) works for P = 0.5 pu and T_A = 9.2 ms, which means less than ½ cycle. The NN_3 (classification) works for P = 0.2 pu and T_A = 21.18 ms, i.e., about one cycle. The successful operational range of each ANN can be observed, which is larger than the one specified during the training process where P = 0.7 pu and R_F = 20 Ω. If the response time is not the main concern, the NN_3 could also be used to assist the detection function, significantly extending the operational range for the algorithm. Overall output could be derived using an OR operator connected at NN_3 outputs (see Fig. 3(a) and Fig. 3(c)), as shown in Fig. 9. Thus, the NN_3 could be used both to classify faults and also as a support to detect three-phase faults at the rectifier side. The range of V_{AC1} (see item b aforementioned) did not significantly affect the algorithm´s performance.

4.2 Double-Phase Fault at the Rectifier Side

After 10 new simulations for each ANN, it was observed that the R_F has a minimal influence on the ANN´s performance, in contrast to P which was observed to significantly affect the ANN's performance. Regarding P, only the NN_3 shows improvements considering the values specified during the training process (0.7 pu). However, with respect to fault resistance, all of them respond to values larger than the one used in the training set (20 Ω). The response time is less than one cycle for NN_2 and NN_3 and slightly longer than one cycle for the NN_1. Depending on the system´s requirements, the ANN_1 could be used in association with others to extend its operational range. As an example, the NN_2 or NN_3 outputs could be used for an OR operator to assist the detection function, as discussed in the previous Subsection 4.1.

4.3 Single-Phase Fault at the Rectifier Side

After 16 new simulations for each ANN, it was observed that the R_F significantly affects the ANN's performance and all the limits are practically the same as the ones used in the training process, unless two of them can work with 25 Ω, against 20 Ω used in the training set.

4.4 Three-Phase Fault at the Inverter Side

After 12 new simulations for each ANN, it was observed that NN_1 and NN_2 are not affected by R_F and they work for P = 0.6 pu and P = 0.5 pu, respectively. Both cases present T_A about a half cycle. The NN_4 is also not affected by R_F and is able to work for P = 0.5 pu, but T_A = 41.05 ms (~ 2 cycles).

4.5 Double-Phase Fault at the Inverter Side

After 12 new simulations for each ANN, it was observed that NN_1 and NN_2 are able to respond to R_F = 50 Ω, whilst the power across the line can be set to P = 0.6 pu and P = 0.5 pu, respectively. The NN_4 is more restricted, as the maximum fault resistance is R_F = 40 Ω and the minimum power across the line is P = 0.7 pu. To classify the type of fault at the inverter side, T_A = 157.80 ms (almost 8 cycles).

4.6 Single-Phase Fault at the Inverter Side

After 16 new simulations for each ANN, a similar behavior was noticed when compared to a single-phase fault at the rectifier side. This means that essentially the training set values were maintained, unless $R_F = 30\ \Omega$ for NN_2.

4.7 DC Transmission Line Fault

For this type of fault, case 36 was selected as the most critical case (see Table 1) and 48 new simulations were applied to each ANN. It could be observed that NN_1 and NN_2 are significantly affected by the power across the line, and the minimum limit permitted is P = 0.7 pu, which is the same used during the training process. However, for fault detection, the NN_1 is able to respond correctly until $R_F = 40\ \Omega$ and for the fault location, NN_2 is able to respond correctly until $R_F = 180\ \Omega$ within $T_A = 29.95$ ms, which represents no more than one and a half cycles. Once again, an association could be made between NN_1 and NN_2 to provide a faster response time and more robust behaviour, i.e., they can work together through an OR operator to extend the fault detection function limits. Fig. 10 presents the NN_2 response time considering different fault resistances for seven different test cases, as follows:

a) Test 1: fault at 150 km, $V_{AC1} = 0.97$ pu, P = 0.98 pu;
b) Test 2: fault at 190 km, $V_{AC1} = 0.97$ pu, P = 0.98 pu;
c) Test 3: fault at 190 km, $V_{AC1} = 0.90$ pu, P = 0.70 pu;
d) Test 4 and 5: fault at 190 km, $V_{AC1} = 1.05$ pu, P = 1.0 pu;
e) Test 6: fault at 5 km, $V_{AC1} = 1.05$ pu, P = 1.0 pu;
f) Test 7: fault at 5 km, $V_{AC1} = 0.90$ pu, P = 0.70 pu.

As can be seen in Fig. 10, the response time increases for higher values of R_F and smaller values of V_{AC1} and P.

4.8 Faults under a Nominal Condition

In this subsection, the ANNs are evaluated when the power system operates under nominal voltage and power condition, as these will be the most common pre fault condition. To carry out this evaluation, the power across the line P and the voltage at the equivalent system at bus 1 V_{AC1} are both fixed to 1 pu. Table 6 shows the average time

for responding to 36 new cases applied to each ANN considering different R_F values (30 Ω, 40 Ω, 50 Ω, and 60 Ω). Confirming the behaviour presented in Table 5, the ANNs respond as expected for a three-phase fault or double-phase fault at the rectifier and inverter sides, even when $R_F = 60$ Ω. Moreover, similar to Table 5, the ANNs respond as expected to single-phase faults on both sides, but they are practically restricted to $R_F = 20$ Ω, used in the training process. With respect to the DC transmission line, it can be noted that the NN_1 is limited to respond correctly for $R_F \leq 50$ Ω, whilst the NN_2 is able to work for $R_F = 60$ Ω, as previously highlighted. According to the times presented, this scheme could be used as the main protection (or a decision support tool) for the rectifier side and DC line, but it is confined as a backup protection considering the inverter side.

5. Conclusions

This work presents a complete scheme based on ANNs to support the protection scheme of VSC based HVDC systems. Using information from the rectifier substation only, the scheme can robustly detect and classify faults at the rectifier side, the inverter side, and the DC transmission line and detect in which of these sections the fault is located. In turn, such a scheme can be used as a decision support tool or as a backup protection. It should be pointed out that the proposed scheme imparts much more information to the protection system compared to conventional methods.

The training methodology developed makes the training process fast and efficient, and independent of the HVDC control system, as only AC and DC data (voltage and current) are used. As discussed in item 3.4 and shown in Fig. 5, by properly adopting three base values and a suitable training set (with representative operational cases), this methodology can be used to defined ANN based decision support tools for other VSC-HVDC systems.

A large number of simulations (202 for each ANN) were used to evaluate the algorithm´s performance and its characteristics. For cases existing within the training space, the expected response was reliably obtained, which indicates that the proposed scheme is completely robust for fault cases within the training space. Moreover, extensive tests showed the limits of the algorithm´s performance lie beyond the range of the training parameters. Other than extending the training data, a number of ways to

increase these performance limits were investigated, such as tuning the counter parameters and combining the outputs of different ANNs by associating them with logic gates.

It should be clear that all benefits reported in this paper are possible without any significant additional costs, as only available signals are used, no communication link is needed, and no special hardware is provided. It means that a more reliable protection system can be achieved, by using practically the available infrastructure.

It is important to state that, at present, most point-to-point DC links are protected by breakers residing on the AC side and in the event of a fault, the entire link is de-energised. The proposed scheme would, therefore, suit existing systems or new systems with future DC breakers with better fault current interrupting capabilities.

6. Acknowledgements

The authors would like to thank the Coordination for the Improvement of Higher Level Personnel (CAPES) and the Ministry of Education of Brazil for its financial support.

7. References

[1] Anderson, P.M.: 'Power System Protection' (McGraw-Hill, 1999).

[2] Kundur, P.: 'Power System Stability and Control' (McGraw-Hill, 1994).

[3] Kimbark, E.W.: 'Direct Current Transmission' (Wiley, 1971, vol. 1).

[4] Zhang, Y., Tai, N., Xu, B.: 'Fault analysis and traveling-wave protection scheme for bipolar HVDC lines', IEEE Trans. Power Del., 2012, **27**,(3), pp. 1583–1591.

[5] Dong, Z.X., Ling, T., Thorp, J.S., *et al.*: 'A transient harmonic current protection scheme for HVDC transmission line', IEEE Trans. Power Del., 2012, **27**, (4), pp. 2278–2285.

[6] Liu, X., Osman, A.H., Malik, O.P.: 'Real-time implementation of a hybrid protection scheme for bipolar HVDC line using FPGA', IEEE Trans. Power Del., 2011, **26**, (1), pp. 101–108.

[7] Liu, X., Osman, A.H., Malik, O.P.: 'Hybrid traveling wave/boundary protection for monopolar HVDC line', IEEE Trans. Power Del., 2009, **24**, (2), pp. 569–578.

[8] Guobing, S., Xu, C., Xinlei, C., *et al.*: 'A fault-location method for VSC-HVDC transmission lines based on natural frequency of current', Elsevier Inter. Journal Elect. Power Ener. Syst., 2014, **63**, pp. 347–352.

[9] Livani, H., Evrenosoglu, C. Y.: 'A single-ended fault location method for segmented HVDC transmission line', Elsevier Elect. Power Syst. Reser., 2014, **107**, pp. 190–198.

[10] Suonan, J., Zhang, J., Jiao, Z., *et al.*: 'Distance protection for HVDC transmission lines considering frequency-dependent parameters', IEEE Trans. Power Del., 2013, **28**, (2), pp. 723–732.

[11] Farshad M., Sadeh, J.: 'A novel fault-location method for HVDC transmission lines based on similarity measure of voltage signals', IEEE Trans. Power Del., 2013, **28**, (4), pp. 2483–2490.

[12] Descloux, J., Raison, B., Curis, J.B.: 'Protection algorithm based on differential voltage measurement for MTDC grids'. 12th IET International Conference on Developments in Power System Protection, Copenhagen, Denmark, 2014, pp. 1–5.

[13] Naidoo, D., Ijumba, N.M.: 'HVDC line protection for the proposed future HVDC systems'. International Conference on Singapore Power System Technology, Singapore, 2004, pp. 1327–1332.

[14] Jovcic, D., Van Hertem, D., Linden, K., *et al.*: 'Feasibility of DC transmission networks'. 2nd IEEE PES International Conference and Exhibition on Innovative Smart Grid Technologies, Manchester, England, 2011, pp. 1–8.

[15] Ramesh, M., Laxmi, A.J.: 'Fault identification in HVDC using artificial intelligence – recent trends and perspective'. International Conference on Power, Signals, Controls and Computation, Thrissur, 2012, pp. 1–6.

[16] Kandil, N., Sood, V.K., Khorasani, K., *et al.*: 'Fault identification in an AC-DC transmission system using neural networks', IEEE Trans. Power Syst., 1992, **7**, pp. 812–819.

[17] Etemadi, H., Sood, V.K., Khorasani, K., *et al.*: 'Neural network based fault diagnosis in an HVDC system'. International Conference on Electric Utility Deregulation and Restructuring and Power Technologies, London, 2000, pp. 209–214.

[18] Lai, L.L., Che, F.N., Chari, T.: 'Fault identification in HVDC systems with neural networks'. International Conference on Advances in Power System Control, Operation and Management, Hong Kong, 1993, pp. 231–236.

[19] Sanjeevikumar, P., Paily, B., Basu, M. *et al.*: 'Classification of fault analysis of HVDC systems using artificial neural network'. International Power Engineering Conference, Romania, 2014, pp. 1–5.

[20] Moshtagh, J., Jannati, M., Baghaee, H.R., *et al.*: 'A novel approach for online fault detection in HVDC converters'. International Middle-East Power System Conference, Aswan, 2008, pp. 307–311.

[21] Narendra, K.G., Sood, V.K., Khorasani, K., *et al.*: 'Application of a radial basis function (RBF) neural network for fault diagnosis in a HVDC system', IEEE Trans. Power Syst., 1998, **13**, (1), pp. 177–183.

[22] Khodaparastan, M., Mobarake, A. S., Gharehpetianand, G. B., *et al.*: 'Smart fault classification in HVDC system based on optimal probabilistic neural networks'. 2nd Iranian Conference on Smart Grids, Iran, ,2012, pp. 1–4.

[23] Abu-Jasser A., Ashour M.: 'Backpropagation Feedforward NN for Fault Detection and Classifying of Overhead Bipolar HVDC TL Using DC Measurements', JERT Journal of Engineering Research and Technology, 2015, **2**, (3), pp. 197–202.

[24] 'MATLAB User's Guide: R2012a Documentation' (MathWorks Inc, 2012).

[25] Khatir, M., Zidi, S.A., Fellah, M.K., *et al.*: 'HVDC Transmission Line Models for Steady-State and Transients Analysis in SIMULINK Environment'. Annual Conference on IEEE Industrial Electronics, Paris, 2006, pp. 436–441.

[26] Marvik, J. I., Svendsen, H. G.: 'Analysis of grid faults in offshore wind farm with HVDC connection', Elsevier Energy., 2013, **35**, pp. 81–90.

[27] Wang, Y., Dinavahi, V.: 'Low-latency distance protective relay on FPGA', IEEE Trans. Smart Grid, 2014, **5**, (2), pp. 896–905.

8. Appendices

Fig. A.1. to Fig. A.4.

Table A.1

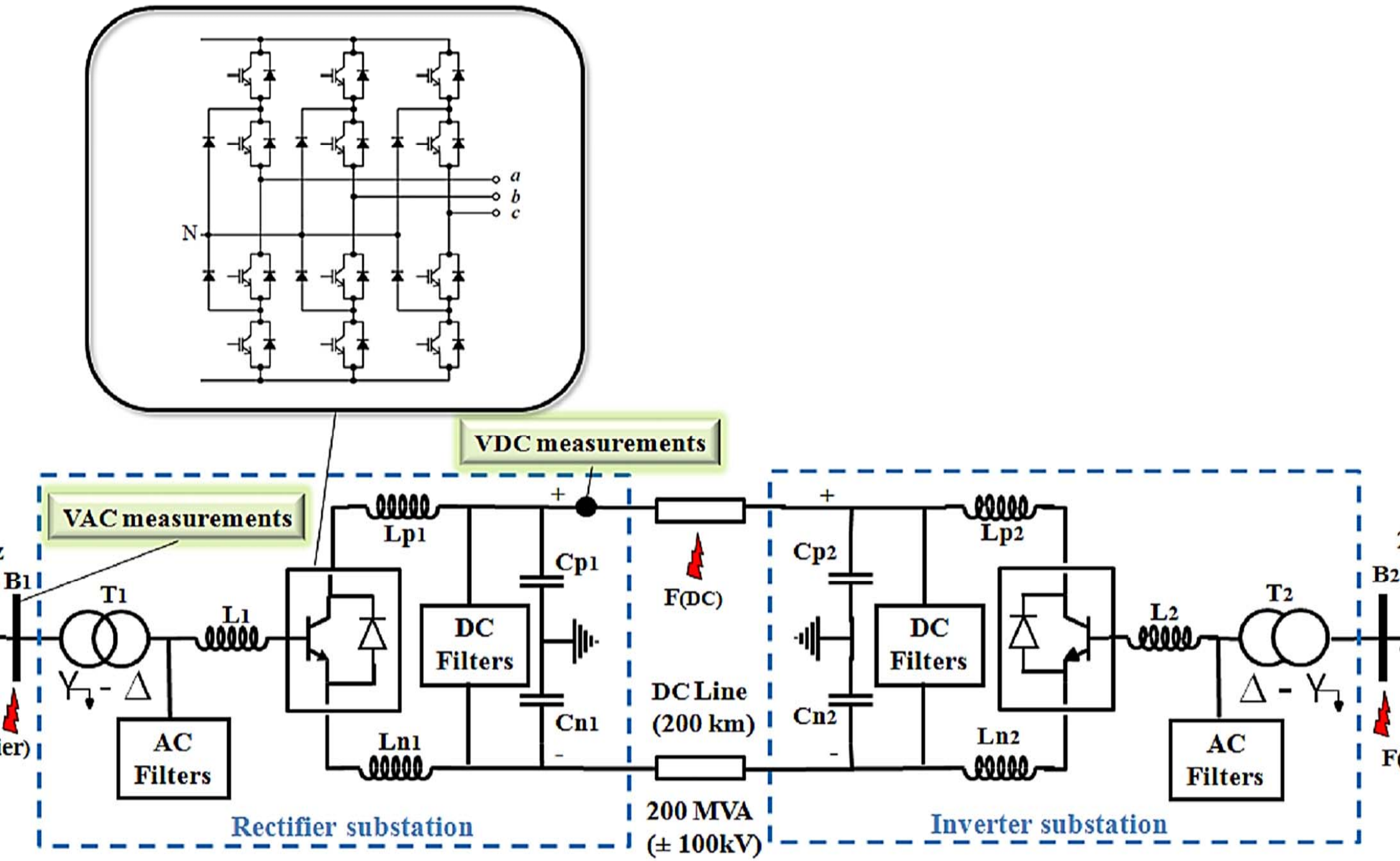

Fig. 1. *Single line diagram of the VSC-HVDC test system.*

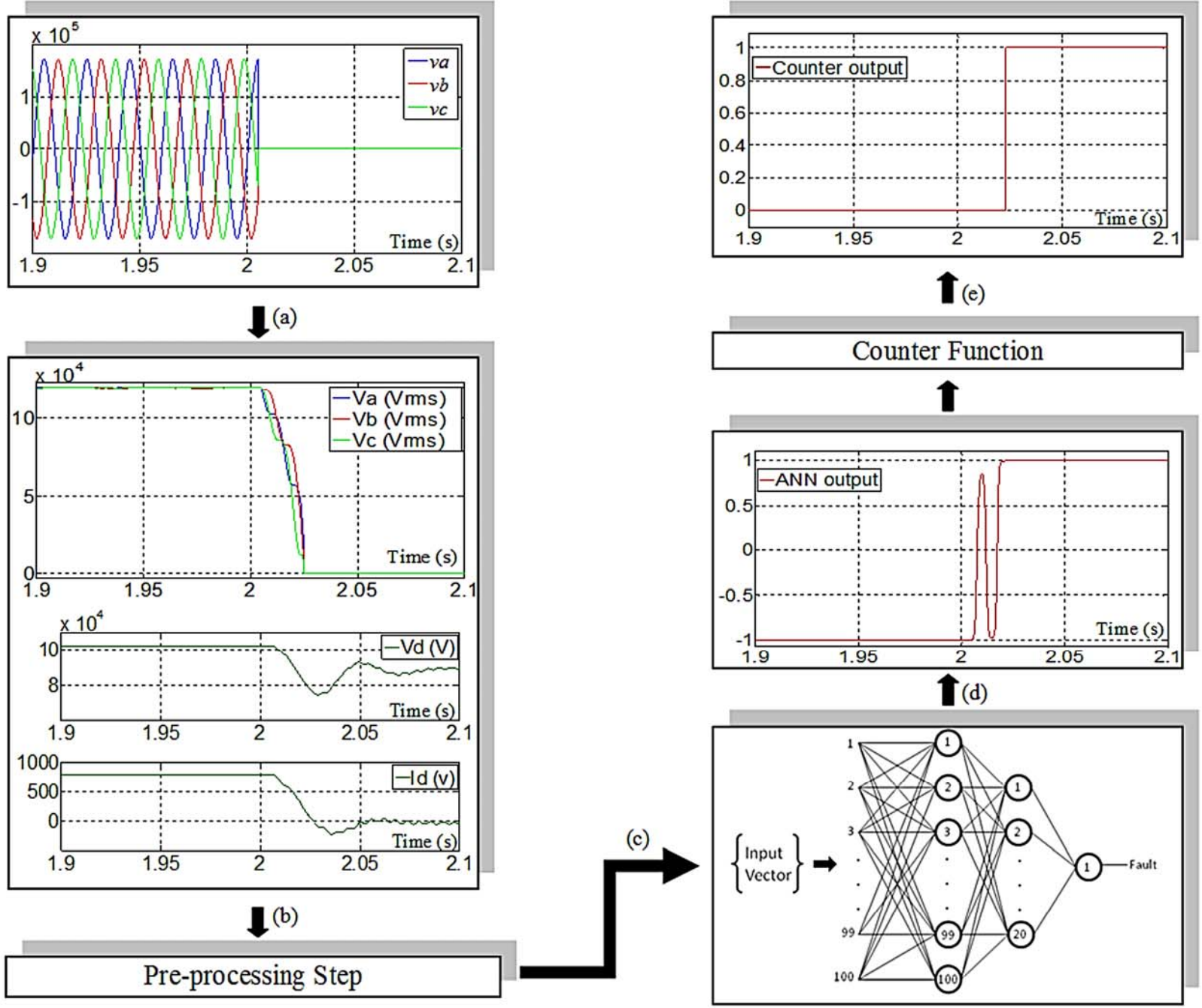

Fig. 2. *Input signals and processing steps. (a) Three-phase voltage at Bus 1, where the fault occurred at 2.005 s; (b) Three-phase RMS voltage and DC values available at the rectifier substation to be applied to the pre-processing tep; (c) ANN for fault detection using information from input vector; (d) ANN output unstable during the transition from pre-fault to post-fault condition; (e) Totally stable counter output .*

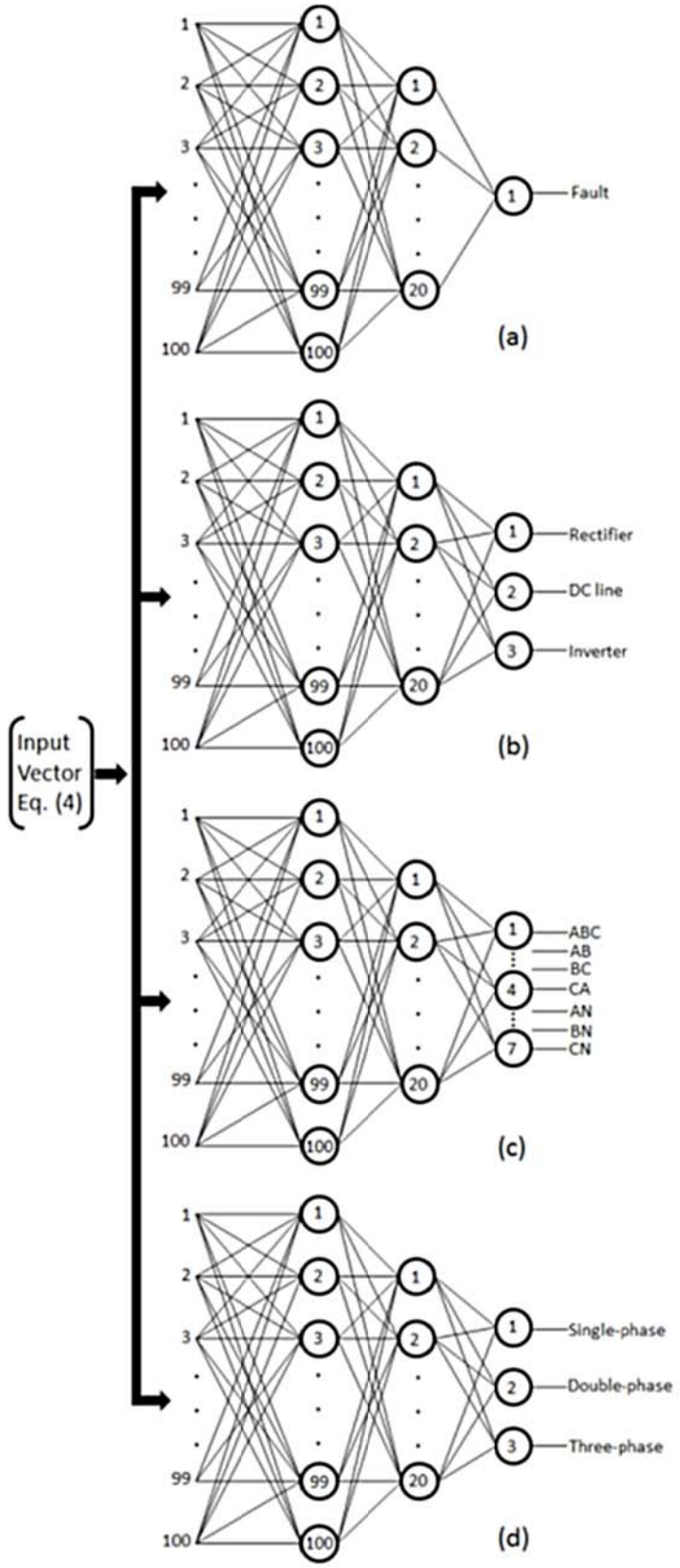

Fig. 3. *ANN considered for: (a) fault detection, (b) section location, (c) fault classification at the rectifier side, and (d) fault classification at the inverter side.*

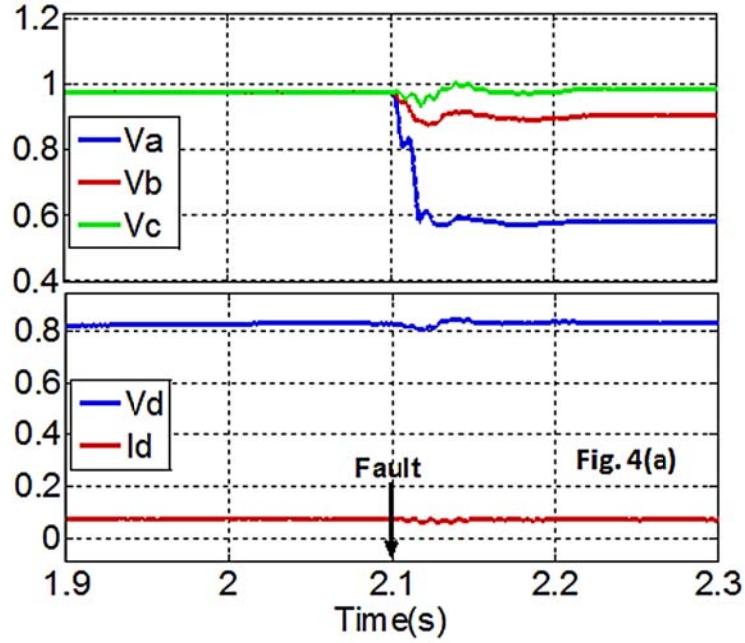

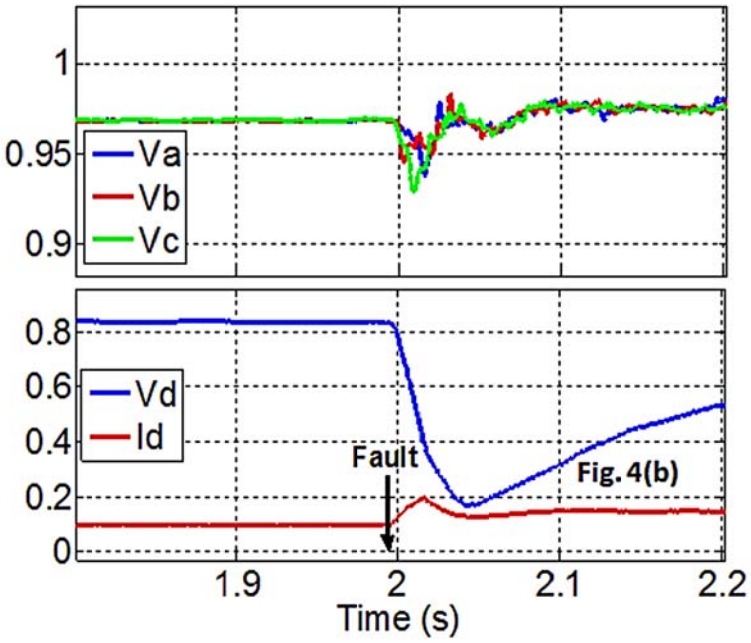

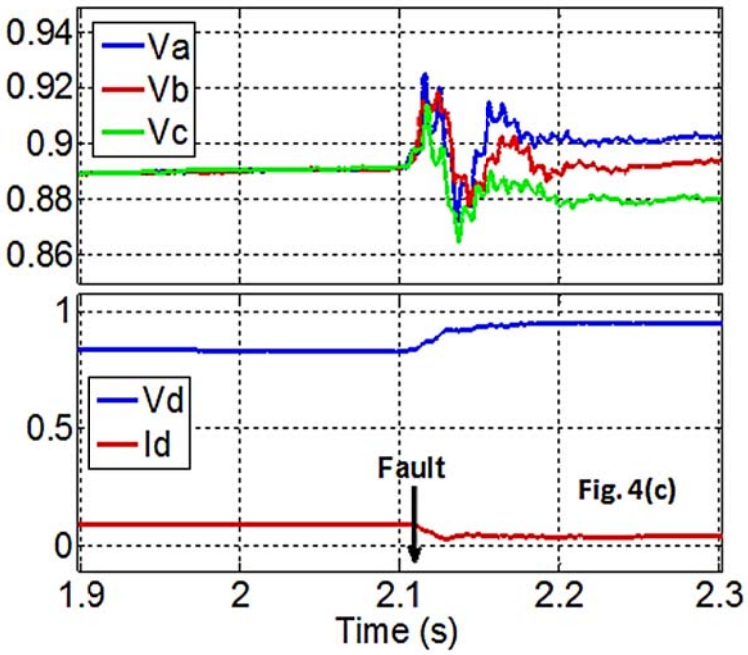

Fig. 4. *Different types and fault locations. (a) Single-phase fault (phase A) at the rectifier substation; (b) Pole-to-ground fault at the DC line; (c) Phase-to-phase fault (phases B and C) at the inverter substation. To find out more about these cases see Table I, cases 12, 16 and 38, respectively.*

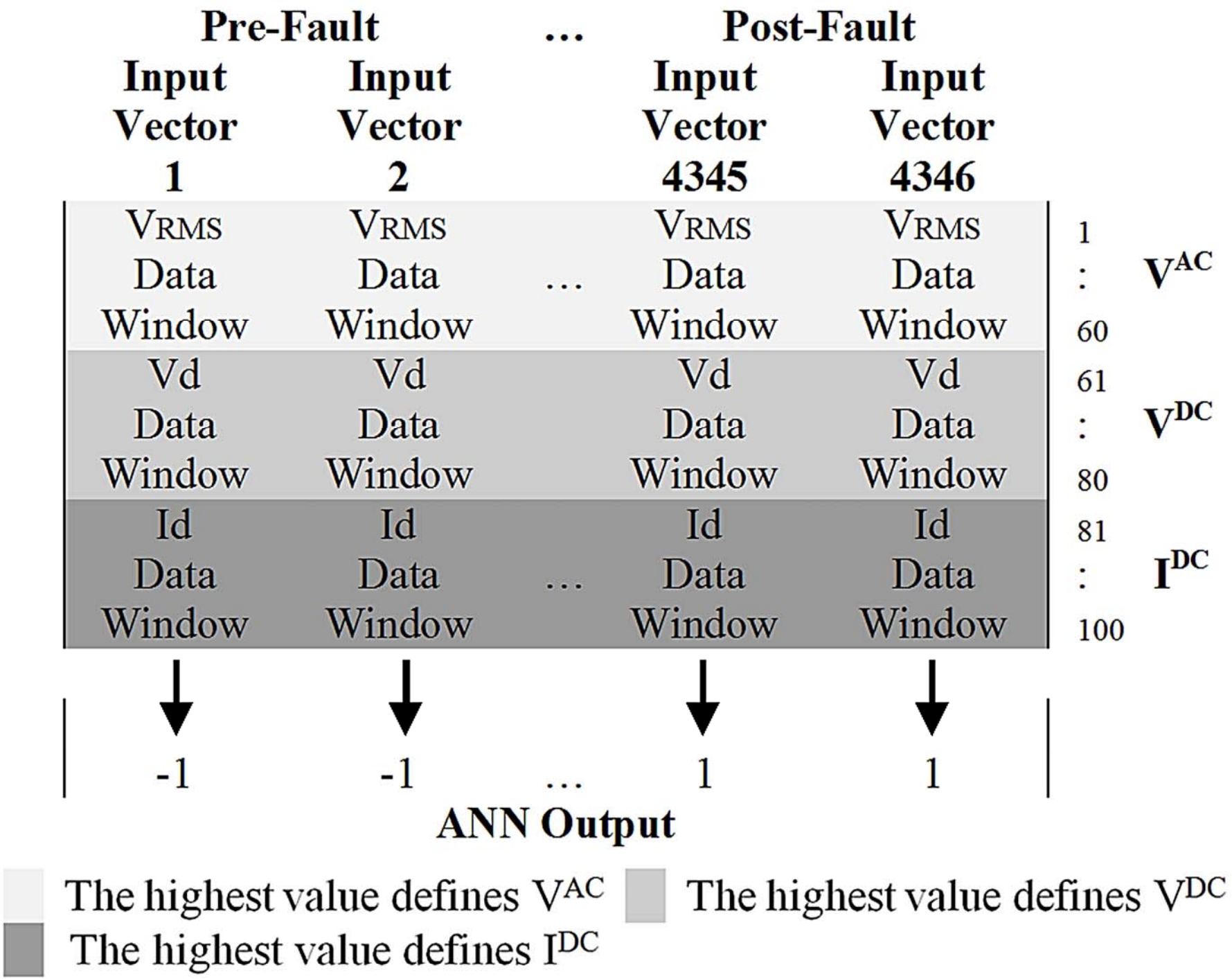

Fig. 5. *Training set used to train the ANN fault detection.*

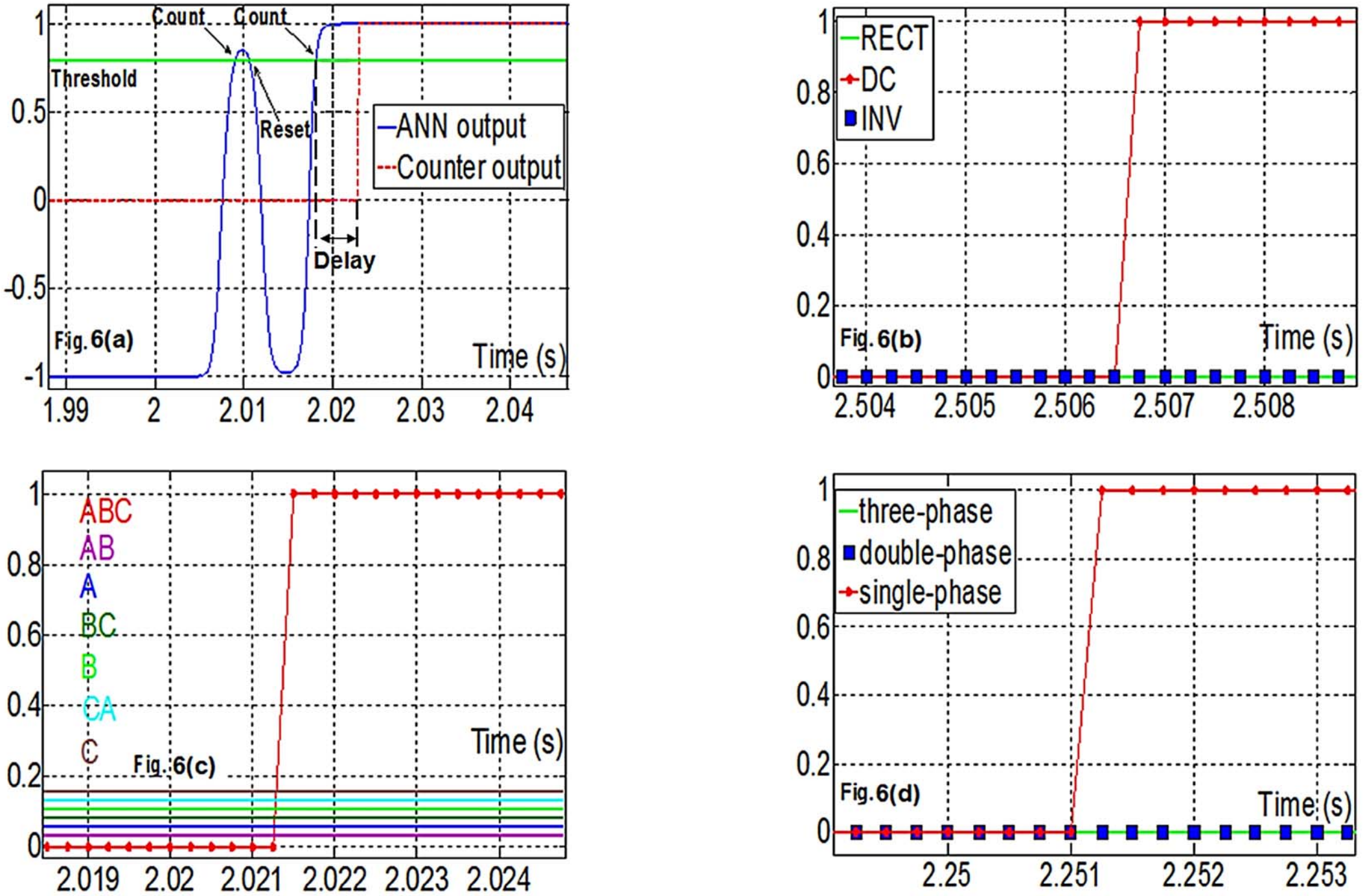

Fig. 6. *Response time analysis of test cases presented in Table 1: (a) case 21, fault at 2.005 s; (b) case 4, fault at 2.5 s; (c) case 33, fault at 2.005 s; (d) case 19, fault at 2.2 s.*

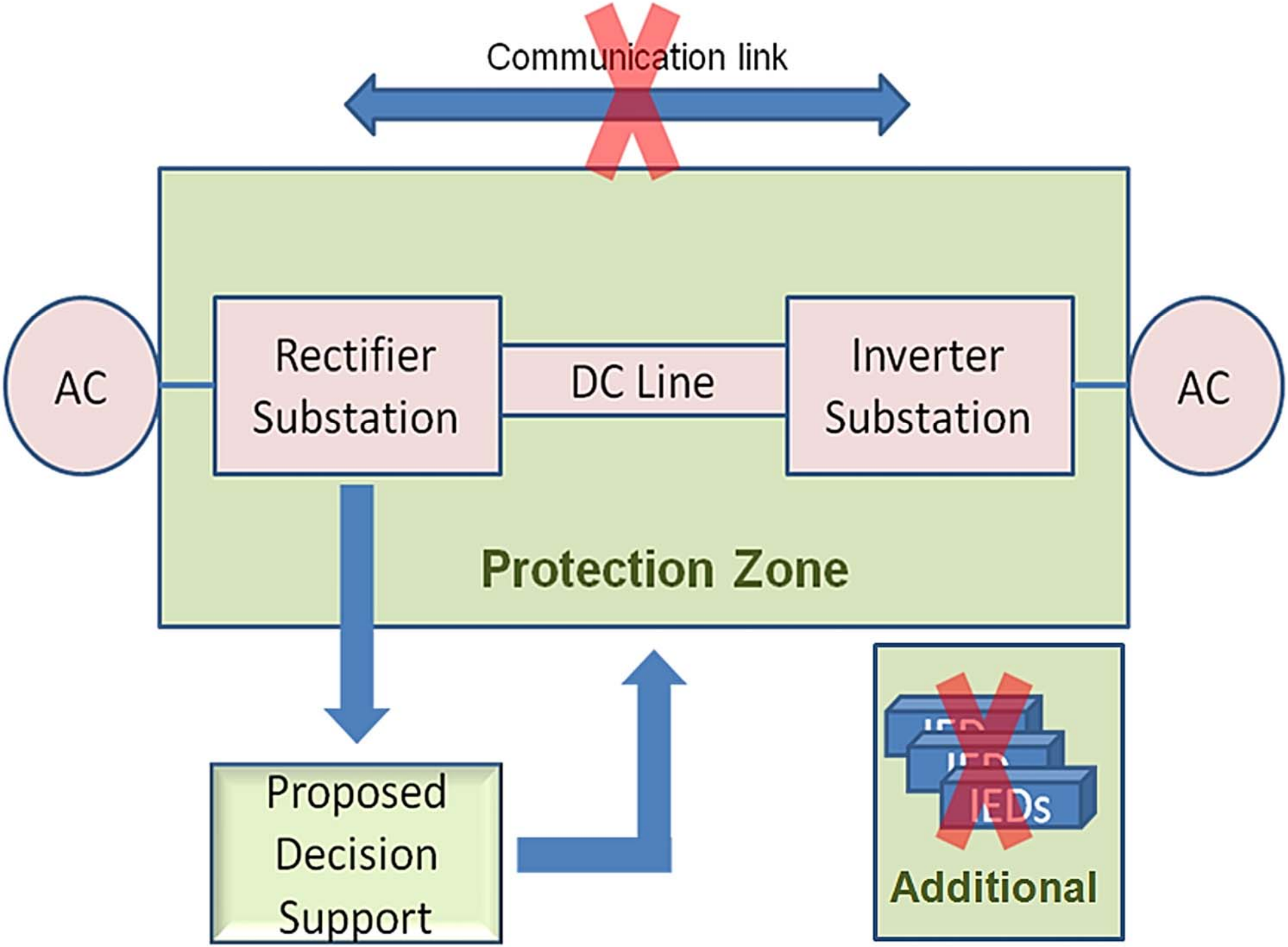

Fig. 7. *Benefits and features of the proposed scheme.*

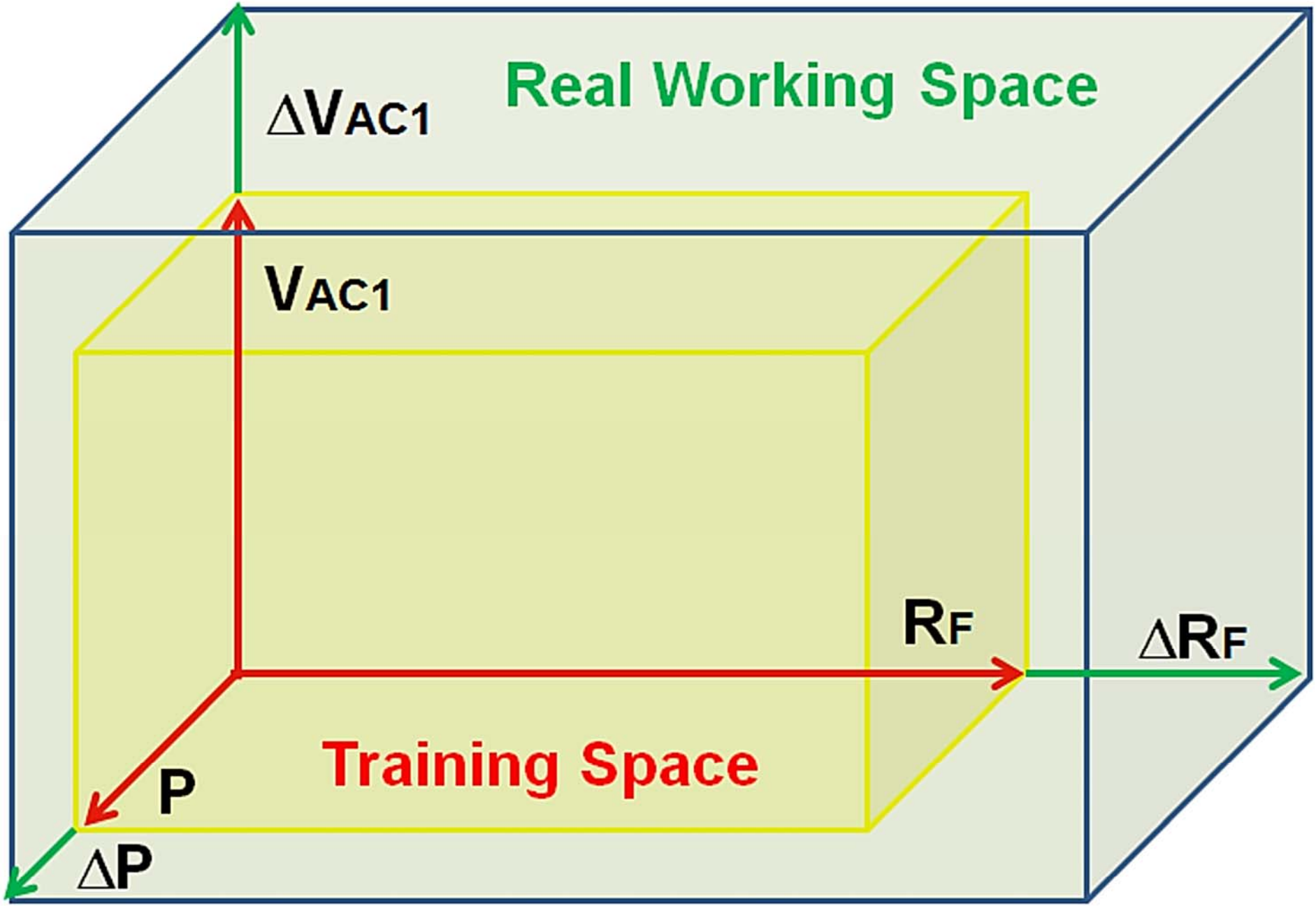

Fig. 8. *Real working space of the proposed scheme.*

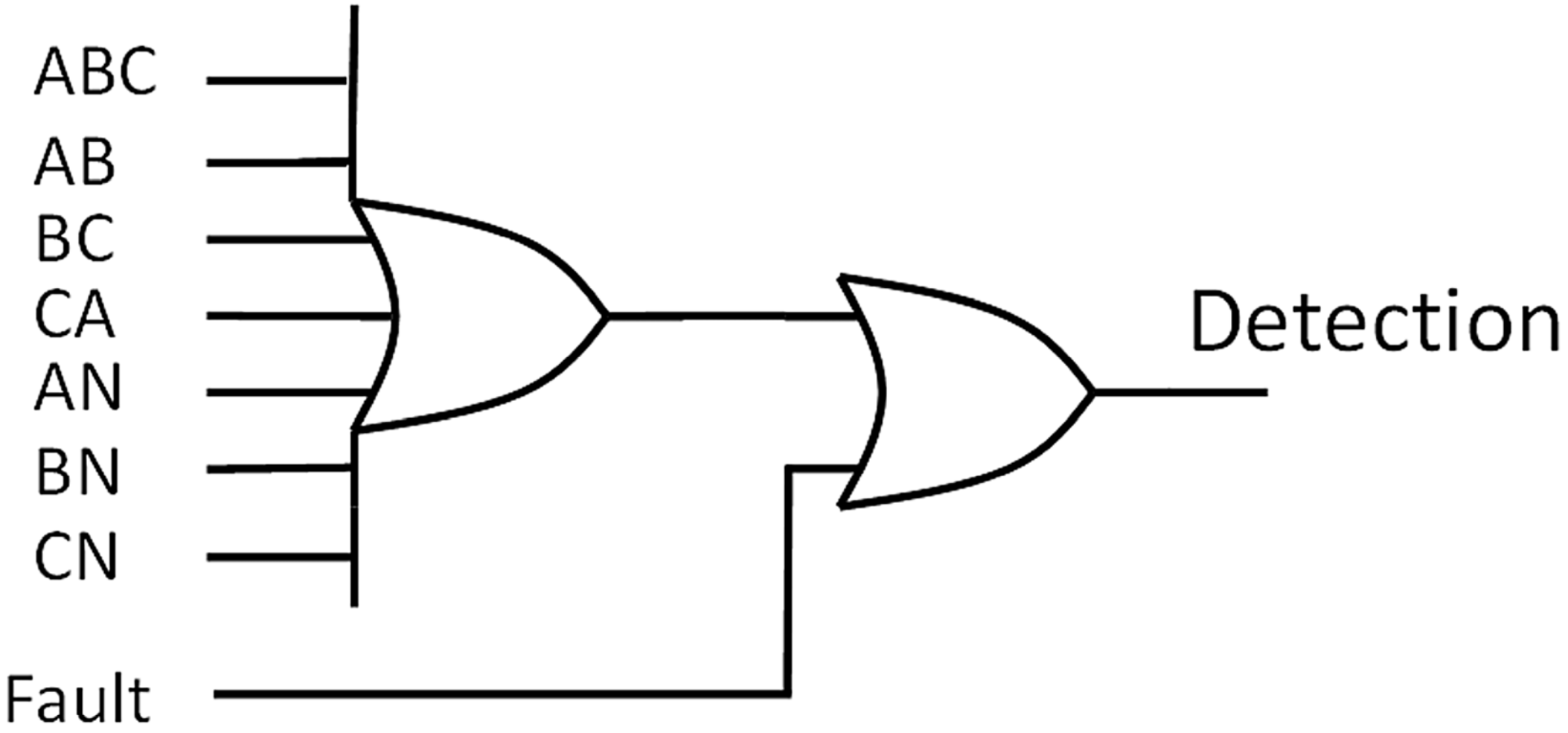

Fig. 9. *Using an OR function to extend the algorithm's limits.*

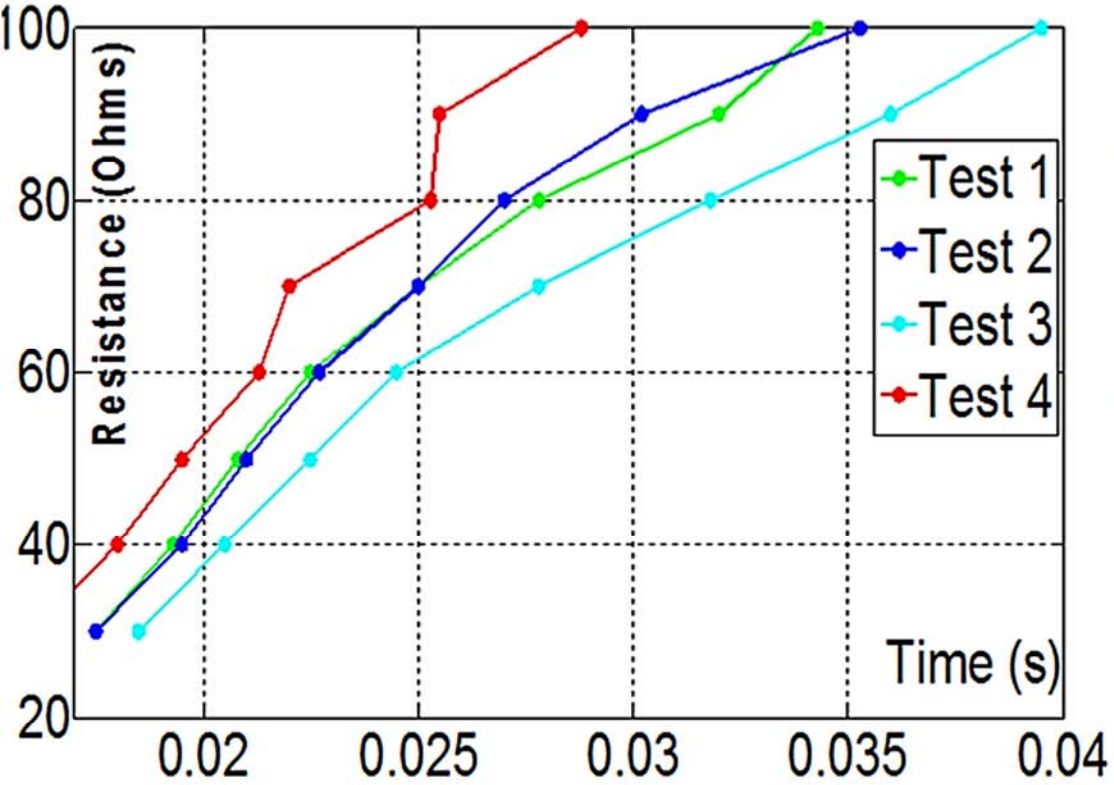

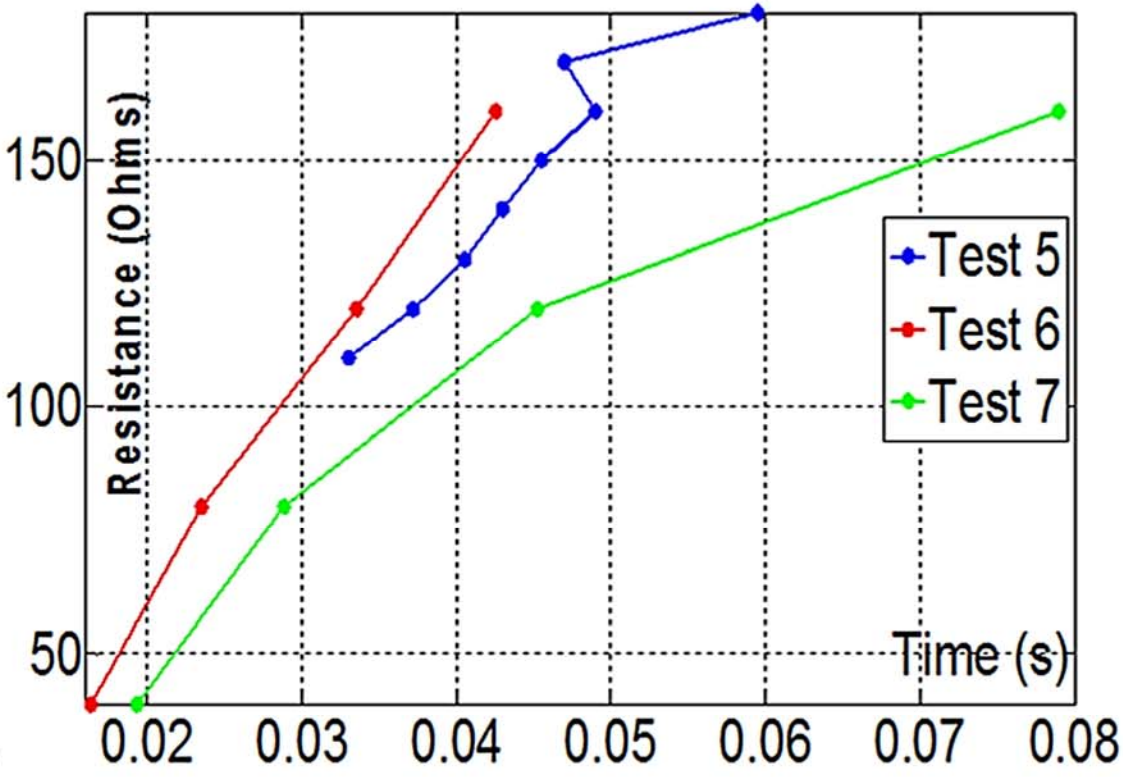

Fig.10. *Location time for DC line faults.*

Table 1 Test Cases and Response Times (ms)

Case	Fault	V_{AC1}	P	R_F	T_D	T_L	T_{CR}	T_{CI}
1-R	ABC	0.92	1	0	21.0	6.50	21.3	X
2-R	B	1	0.85	0	31.0	18.2	15.3	X
3-R	BC	1	1	10	34.0	12.8	19.5	X
4-D	0%	0.95	0.82	0	14.0	6.70	X	X
5-D	25%	1	0.95	5	18.0	10.3	X	X
6-D	75%	1	0.95	5	18.5	10.8	X	X
7-D	100%	1	0.8	10	20.8	12.8	X	X
8-I	AC	0.9	0.9	5	5.00	11.5	X	(1)
9-I	C	0.97	0.9	10	18.7	17.3	X	51.5
10-I	ABC	0.95	0.87	10	10.5	10.5	X	32.0
11-R	ABC	0.9	0.95	20	21.5	7.50	21.0	X
12-R	A	1	0.75	18	29.5	27.3	16.8	X
13-R	AC	0.92	0.7	25	3.80	7.00	15.5	X
14-D	0%	0.9	0.8	20	28.3	14.8	X	X
15-D	25%	0.96	0.75	22	27.0	15.0	X	X
16-D	75%	1	1	25	28.0	15.8	X	X
17-D	100%	0.98	0.7	15	23.3	14.5	X	X
18-I	BC	0.9	0.75	15	13.8	13.8	X	86.0
19-I	B	0.9	0.9	20	18.5	17.8	X	51.3
20-I	ABC	0.9	0.7	15	9.50	9.80	X	31.8
21-R	ABC	0.92	0.85	15	18.0	6.30	21.0	X
22-R	B	0.95	0.8	8	33.5	17.8	16.0	X
23-R	BC	0.96	0.77	20	15.5	11.8	19.5	X
24-D	0%	0.97	0.79	16	23.0	13.5	X	X
25-D	25%	1	0.95	15	21.8	12.8	X	X
26-D	75%	0.96	0.89	3	18.5	10.8	X	X
27-D	100%	0.98	0.98	9	21.0	12.5	X	X
28-I	AC	0.99	0.79	8	13.5	13.3	X	89.2
29-I	C	1.01	0.92	15	21.0	19.3	X	53.2
30-I	ABC	0.95	1	12	11.5	11.3	X	30.8
31-R	ABC	1.02	0.85	18	21.0	10.0	21.3	X
32-R	A	1	0.77	16	29.0	19.8	16.5	X
33-R	AC	1.05	0.75	22	18.3	14.5	16.5	X
34-D	0%	0.95	0.85	15	23.3	13.5	X	X
35-D	25%	1.04	0.85	23	24.3	14.3	X	X
36-D	75%	0.97	0.98	25	30.2	16.0	X	X
37-D	100%	1.03	0.75	18	23.3	14.5	X	X
38-I	BC	0.9	0.76	17	15.0	15.0	X	86.5
39-I	B	1.05	0.93	20	23.8	21.0	X	54.0
40-I	ABC	1.04	0.75	19	11.5	11.5	X	53.0

R = Rectifier side; D = DC Line; I = Inverter side.

(1) = A single-phase fault was indicated before the double-phase fault.

X = Not applicable.

Table 2 Counter Settings

	T_D	T_L			T_{CR}	T_{CI}		
		R	D	I	All 7 outputs	1ϕ	2ϕ	3ϕ
N	20	20	20	20	20	160	160	40
V	0.8	0.8	0.8	0.8	0.8	0.8	0.8	0.8

For a sample rate of 4 kHz, N (20 samples) is equal to 5 ms.

Table 3 Improved Approach - Test Cases and response Time (ms)

Case	Fault	V_{AC1}	P	R_F	T-1ϕ	T-2ϕ	T-3ϕ	T_{CI}
8-I	AC	0.9	0.9	5	∞	89.5	∞	(1)
9-I	C	0.97	0.9	10	62.0	∞	∞	51.5
10-I	ABC	0.95	0.87	10	∞	∞	29.3	32.0
18-I	BC	0.9	0.75	15	∞	71.0	∞	86.0
19-I	B	0.9	0.9	20	62.0	∞	∞	51.3
20-I	ABC	0.9	0.7	15	∞	∞	29.0	31.8
28-I	AC	0.99	0.79	8	∞	42.0	∞	89.2
29-I	C	1.01	0.92	15	63.3	∞	∞	53.2
30-I	ABC	0.95	1	12	∞	∞	28.5	30.8
38-I	BC	0.9	0.76	17	∞	71.0	∞	86.5
39-I	B	1.05	0.93	20	64.0	∞	∞	54.0
40-I	ABC	1.04	0.75	19	∞	∞	30.2	53.0

T-1ϕ, T-2ϕ, T-3ϕ = single-phase, double-phase, and three-phase ANN.
(1) = A single-phase fault was indicated before the double-phase fault.

Table 4 Improved Approach - Counter Settings

	Independents ANN		
	T-1ϕ	**T-2ϕ**	**T-3ϕ**
N	200	80	30
V	0.9	0.9	0.9

Table 5 Algorithm's Limits

		Rectifier			Inverter			DC
		3ϕ	**2ϕ**	**1ϕ**	**3ϕ**	**2ϕ**	**1ϕ**	
NN_1	**R_F**	∞	60	25	∞	50	20	40
	P	0.65	0.7	0.7	0.6	0.6	0.7	0.7
	T_A	15.92	28.47	33.75	10.94	14.77	20.77	42.64
NN_2	**R_F**	∞	60	20	∞	50	30	180
	P	0.5	0.7	0.7	0.5	0.5	0.7	0.7
	T_A	9.2	10.97	18.25	11.63	16.08	20.16	29.95
NN_3	**R_F**	∞	60	25	X	X	X	X
	P	0.2	0.4	0.7	X	X	X	X
	T_A	21.18	16.22	20.53	X	X	X	X
NN_4	**R_F**	X	X	X	∞	40	20	X
	P	X	X	X	0.5	0.7	0.7	X
	T_A	X	X	X	41.05	157.8	62.82	X

NN_1: Fault detection; NN_2: Fault location; NN_3: Fault classification at the rectifier side; NN_4: Fault classification at the inverter side: R_F: Fault resistance (Ω); T_A: Average time for responding (ms); X: Not applicable.

Table 6 Average time for Responding in Nominal Operation (ms)

	Rectifier			Inverter			DC
	3ϕ	**2ϕ**	**1ϕ**	**3ϕ**	**2ϕ**	**1ϕ**	
NN_1	21.50	33.34	20.8[A]	12.0	16.80	25.3[B]	39.8[C]
NN_2	9.0	13.35	16.1[A]	11.50	16.30	23.2[D]	29.95
NN_3	21.0	16.50	26.5[B]	X	X	X	X
NN_4	X	X	X	28.30	82.10	52.5[A]	X

[A]: Limited to training set value R_F = 20 Ω; [B]: maximum R_F = 30 Ω;
[C]: maximum R_F = 50 Ω; [D]: Maximum R_F = 40 Ω; X: Not applicable.

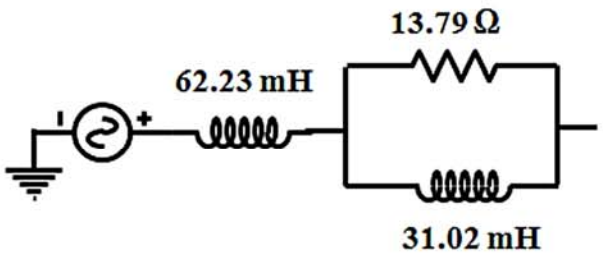

Fig. A.1. *AC system connected at Bus 1.*

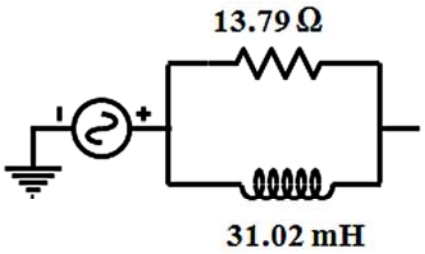

Fig. A.2. *AC system connected at Bus 2.*

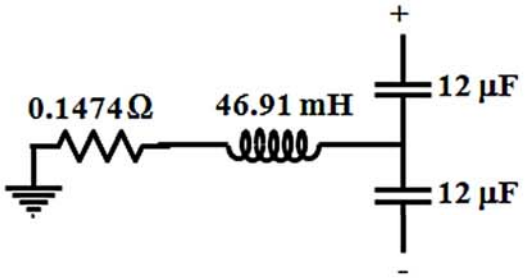

Fig. A.3. *AC filters at the rectifier and inverter substations.*

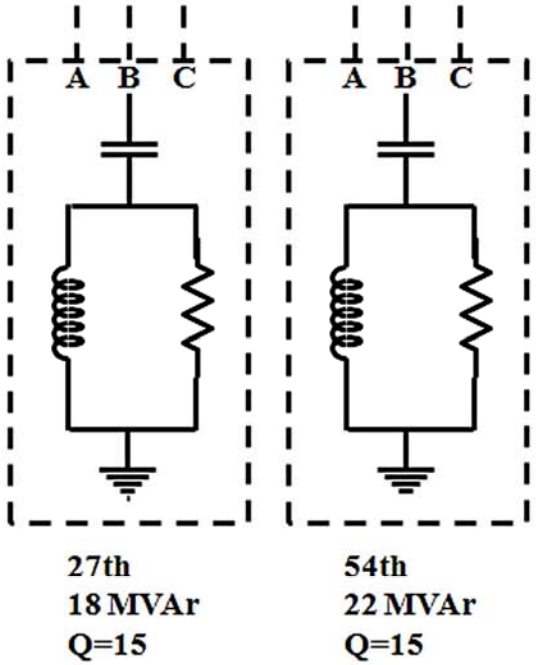

Fig. A.4. *DC filters at the rectifier and inverter substations.*

TABLE A.1 VSC-HVDC PARAMETERS

Component	Value
L1	23.9 mH
Lp1	8 mH
Ln1	8 mH
Cp1	70 μF
Cn1	70 μF
T1	200 MVA - 230:100 kV
L2	23.9 mH
Lp2	8 mH
Ln2	8 mH
Cp2	70 μF
Cn2	70 μF
T2	200 MVA - 100:230 kV